Flow regime classification in air–magnetic fluid two-phase flow

2008 J. Phys.: Condens. Matter 20 204141

(http://iopscience.iop.org/0953-8984/20/20/204141)

IOP Publishing Journal of Physics: Condensed Matter

J. Phys.: Condens. Matter **20** (2008) 204141 (6pp) doi:10.1088/0953-8984/20/20/204141

Flow regime classification in air–magnetic fluid two-phase flow

T Kuwahara[1,2], F De Vuyst[1] and H Yamaguchi[2]

[1] Ecole Centrale Paris, Laboratoire Mathématiques Appliquées aux Systèmes, Grande Voie des Vignes 92295 Châtenay-Malabry, France
[2] Department of Mechanical Engineering, Doshisha University, 1-3 Tataramiyakodani, Kyotanabe-shi, Kyoto 610-0321, Japan

E-mail: takuya.kuwahara@gmail.com (T Kuwahara)

Received 5 April 2008
Published 1 May 2008
Online at stacks.iop.org/JPhysCM/20/204141

Abstract

A new experimental/numerical technique of classification of flow regimes (flow patterns) in air–magnetic fluid two-phase flow is proposed in the present paper. The proposed technique utilizes the electromagnetic induction to obtain time-series signals of the electromotive force, allowing us to make a non-contact measurement. Firstly, an experiment is carried out to obtain the time-series signals in a vertical upward air–magnetic fluid two-phase flow. The signals obtained are first treated using two kinds of wavelet transforms. The data sets treated are then used as input vectors for an artificial neural network (ANN) with supervised training. In the present study, flow regimes are classified into bubbly, slug, churn and annular flows, which are generally the main flow regimes. To validate the flow regimes, a visualization experiment is also performed with a glycerin solution that has roughly the same physical properties, i.e., kinetic viscosity and surface tension, as a magnetic fluid used in the present study. The flow regimes from the visualization are used as targets in an ANN and also used in the estimation of the accuracy of the present method. As a result, ANNs using radial basis functions are shown to be the most appropriate for the present classification of flow regimes, leading to small classification errors.

(Some figures in this article are in colour only in the electronic version)

1. Introduction

In studies on gas–liquid two-phase flow, determination of the flow regime (flow pattern) is one of the key parts since the flow characteristics strongly depend on it. Therefore, identifications of the flow regime are important. In general, we can observe four main flow regimes in vertical upward gas–liquid two-phase flows, as shown in figure 1. There is no consistent theory on flow regime classification so it is not easy to estimate flow regimes using theoretical approaches. As for experimental methods, a number of methods have been proposed (see e.g. [1, 2]). Most of the methods are contact methods, namely requiring contact with the flow of interest. Even in non-contact methods, the cost of deployment and measurement is often significant. Some pipe processing is also often needed. The ideal method is flow regime classification based on an easy and non-contact measurement.

Applications of magnetic fluids using gas–liquid flow have been proposed, such as in energy conversion devices and heat transport devices [3, 4]. For the analysis of these devices, flow regimes are also important for the aforementioned reason. However, flow regime classification in magnetic fluids is much more difficult since magnetic fluids are opaque. In the present work, a new flow regime method of classification of air–magnetic fluid two-phase flows based on non-contact measurement using artificial neural networks as classification tools has been proposed.

2. Experiment

2.1. Principle of measurement

Figure 2 shows the process schematic for the present measurement. In the system under consideration, a uniform alternating magnetic field is applied to a pipe by an excitation

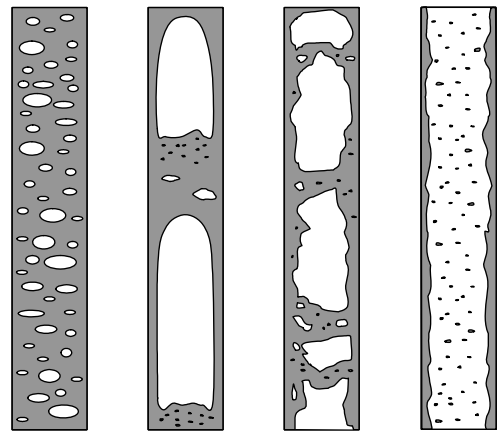

Figure 1. Flow regimes in upward vertical gas–liquid two-phase flow.

coil which is a Helmholtz coil. An air–magnetic fluid mixture flows in the pipe. In this situation, when directions of the magnetic field and magnetization of the magnetic fluid are parallel, the magnetic flux density $\boldsymbol{B}_{\mathrm{mix}}$ passed through the magnetic fluid which includes gaseous phases is expressed as [5]

$$\boldsymbol{B}_{\mathrm{mix}} \approx \mu_0\{\boldsymbol{H} + (1-\alpha)\boldsymbol{M}_{\mathrm{mf}}\} \tag{1}$$

where $\boldsymbol{H}$ is the applied magnetic field, μ_0 is the vacuum permeability, α is the void fraction and $\boldsymbol{M}_{\mathrm{mf}}$ is the magnetization of the magnetic fluid. For the water-based magnetic fluid which is used in the present study, equation (1) works well within an error of 1.37%. The induced electromotive force that occurs in the induction coil with n windings in figure 2 is given by employing Faraday's law as

$$V = -n\frac{\partial}{\partial t}\int\int_S \boldsymbol{B}_{\mathrm{mix}} \cdot \mathrm{d}\boldsymbol{S} \tag{2}$$

where S is the inner area of an induction coil. The magnetization of the magnetic fluid is generally expressed by

$$M_{\mathrm{mf}} = n_0 m L\left(\frac{\mu_0 m H}{kT}\right) \tag{3}$$

where n_0 is the number of magnetic particles per unit volume, m is the magnetic moment of a magnetic particle, k is Boltzmann's constant and T is the temperature. The function $L(\cdot)$ stands for the Langevin function $L(\xi) := \coth\xi - \xi^{-1}$. In consideration of equations (1)–(3), when the applied magnetic field and the temperature is constant, the induced electromotive force is uniquely determined by the void fraction. When gaseous phases (bubbles) pass through the control volume of the measurement (see figure 2), the void fraction increases, that is, the induced electromotive force decreases. Taking into account this phenomenon and the flow regimes in figure 1, the relations between the flow regimes and the corresponding signal waveform should be as shown in figure 3.

To obtain the characteristics of the signals, the signal waveforms are firstly extracted using a wavelet transform. The

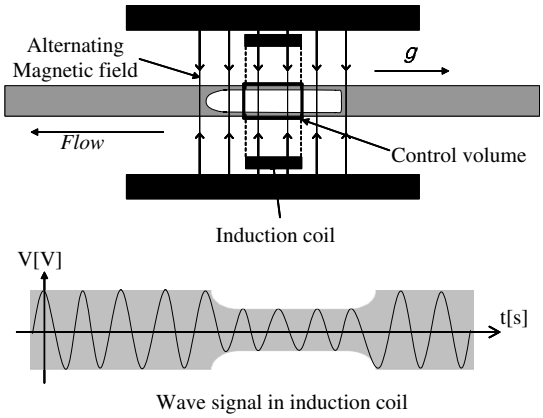

Figure 2. Process schematic for the present measurement.

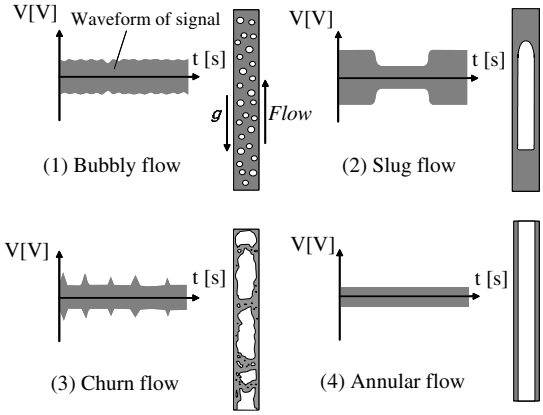

Figure 3. Signal waveforms and flow regimes.

extracted signals are transformed into appropriate input vectors for an artificial neural network (ANN). A low-dimensional voltage distribution was used as ANN input vector. A set of training data, i.e., a set of 'input vectors and targets' assembles an ANN that can classify the flow regimes. More details of data (signal) analysis are mentioned below.

2.2. Test fluid

A water-based magnetic fluid (Taiho Industries Co., Ltd: W-40) was used as the working fluid. The magnetization of the magnetic fluid has low dependence on temperature. In the visualization experiment used to verify the flow regimes, a glycerin solution that has roughly the same kinetic viscosity and surface tension as the water-based magnetic fluid was used. The kinetic viscosity is 13.42×10^{-6} m^2 s^{-1} and the surface tension is 38.90 mN m^{-1}.

2.3. Experimental setup and method

Figure 4 shows the experimental setup for the measurement. The water-based magnetic fluid is made to run in the clockwise direction by a pump. The inner diameter of the pipe is 12 mm. Air injectors, which are connected to an air compressor, are positioned at the lower part of the measuring section. The

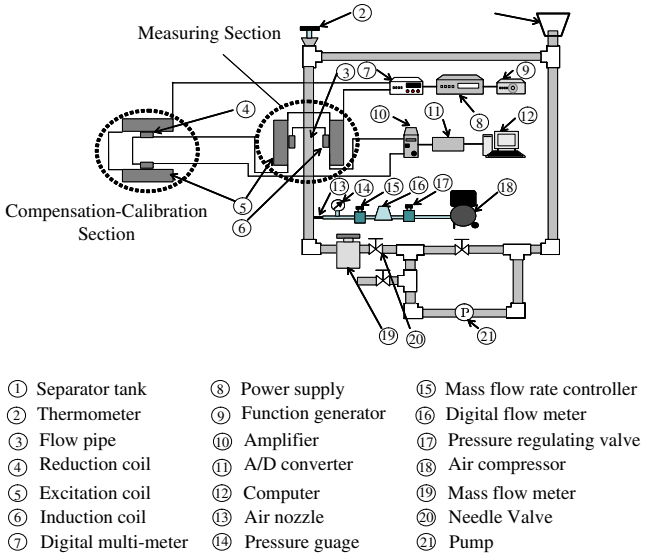

Figure 4. Experimental setup.

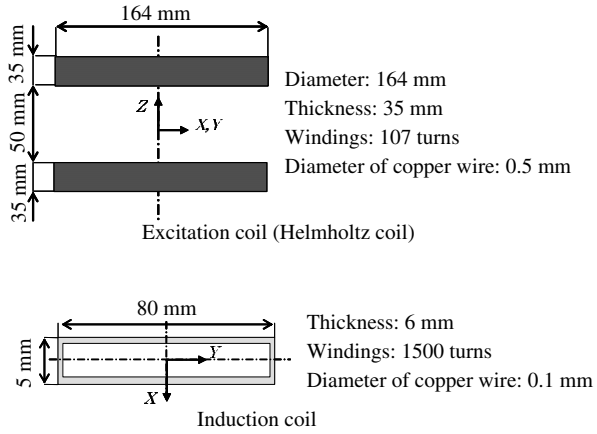

Figure 5. Excitation coil and induction coil (flow in X direction).

Table 1. Flow conditions in the experiment.

Volumetric flux of liquid phase j_l (m s^{-1})	Volumetric flux of gaseous phase j_g (m s^{-1})
0	0–14.737
0.042	0–0.486
0.105	0–0.295

system achieves a vertical upward air–magnetic fluid two-phase flow. The gaseous phases are removed in the separator tank so that the magnetic fluid without the gaseous phases recirculates. The volumetric flux (flow rate per unit area of cross section (m s^{-1})) in each phase can be regulated. The measuring apparatus is located at the measuring section in figure 4. The details of the excitation coil (Helmholtz coil) and induction coil are presented in figure 5. The induction coil is connected to a PC equipped an analog–digital converter (A/D converter) whose the range of input voltage is ± 10 V and the resolution level is 16 bits. The induced electromotive force obtained is achieved by an amplifier installed between the induction coil and the A/D converter. It is noted that time response in the data acquisition system is 10^{-5} s. The sampling frequency is 10 000 Hz and the total number of samplings is 50 000, namely the measuring time is 5 s long. The gain of the amplifier is 1000. The compensation–calibration section consists of the same arrangement of the coils as for the measuring section. The reduction coil in figure 4 is the same as the induction coil. This section is set to cancel the excess electromotive force generated by the induction coil. The excess electromotive force is detected as a base voltage not caused by the magnetization of the magnetic fluid but merely due to the inductance of the coil itself. The magnetic flux density at the applied uniform alternating magnetic field is 0.99 mT with 100 Hz. Table 1 shows the flow conditions in the experiment. The flow condition is determined by considering the removability of the gaseous phases in the separator tank. The experiment with the volumetric flux of liquid phase being 0 m s^{-1} covers all flow regimes, i.e., from bubbly to annular flows. The experiments with the volumetric flux of liquid phase being 0.042 and 0.105 m s^{-1} cover from bubbly to slug flows. The temperature of the magnetic fluid is kept to $22.0 \pm 1.0\,^{\circ}$C in the experiment. The visualization to verify the flow regimes is also conducted with a glycerin solution, which has the same kinetic viscosity and surface tension as the water-based magnetic fluid, in the same manner as in the experiment with the magnetic fluid. The flow regimes determined by the visualization are used for data in an ANN.

Figure 6 shows the representative signal obtained in each flow regime. We can see that the waveforms of the signals obtained agree with the waveforms in figure 3.

3. Data analysis

The signal of the electromotive force obtained in the experiment is processed by a time–frequency analysis using wavelet transforms. Figure 7 presents the signal processing. Firstly the continuous wavelet transform is applied to the signal obtained with the complex Morlet wavelet to extract the waveforms (see figures 7(a) and (b)), namely [6, 7]

$$\mathcal{W}f(a,b) := \int_{-\infty}^{\infty} f(x)\frac{1}{\sqrt{a}}\psi^*\left(\frac{x-b}{a}\right)\mathrm{d}x, \quad \psi(x) \in L^1(\mathbb{R}) \tag{4}$$

where $\mathcal{W}f(a,b)$ stands for the wavelet transform of function $f(x)$ with the scale a and the shift b. The function $f(x)$ is the signal obtained in this case and x is the time or the data position. $\psi^*(x)$ stands for the complex conjugate of $\psi(x)$ which is the mother wavelet and the complex Morlet wavelet is given by

$$\psi(x) = \frac{1}{\sqrt{\pi\gamma_b}}\mathrm{e}^{2\pi\mathrm{i}\gamma_c x}\mathrm{e}^{-\frac{x^2}{\gamma_b}} \tag{5}$$

where γ_b is the bandwidth parameter (=1) and γ_c is the wavelet center frequency (=1.5). The optimal scale a is the maximum value of the coefficient of the wavelet transform. In the present study, the optimal scale level is 150, that is, the extracted signal is

$$f_{\mathrm{ext}}(x) = |\mathcal{W}f(150,b)|. \tag{6}$$

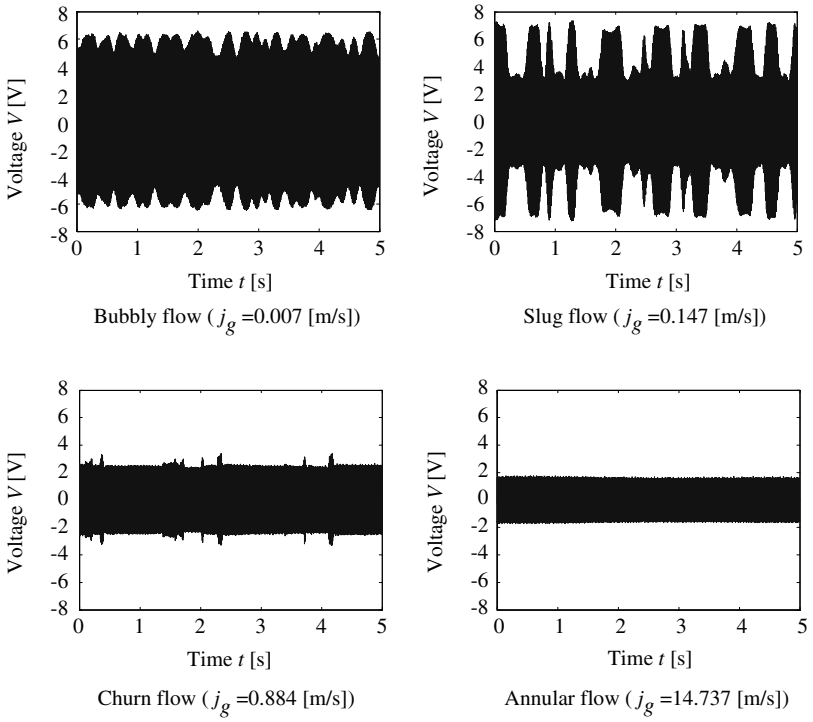

Figure 6. Examples of measured signals for each flow regime ($j_l = 0$ (m s^{-1})).

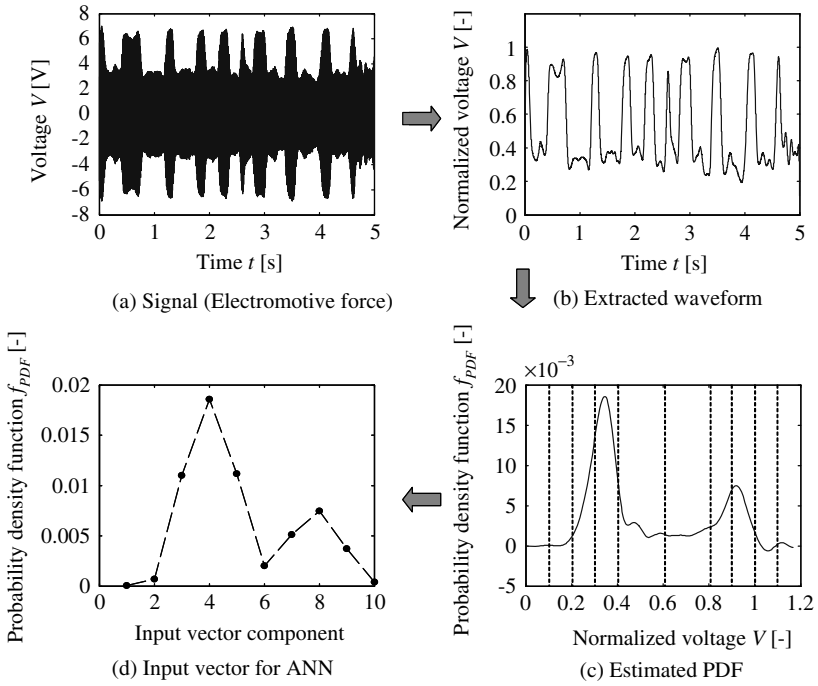

Figure 7. Procedure of signal processing.

The extracted signal is normalized by using the electromotive forces of vacuum (void fraction $\alpha = 1$) and the magnetic fluid without gaseous phases (void fraction $\alpha = 0$).

The normalized signal is transformed into a histogram made of 300 bins. On the basis of the series of the data in each bin, a probability density function (PDF) is estimated using a discrete wavelet transform. Suppose that the PDF is searched for on the whole real axis, belonging to $L^2(\mathbb{R})$. Then it can be expressed by

$$f_{\mathrm{PDF}}(x) = \sum_{k\in\mathbb{Z}} \tilde{c}_k^{(L)} \phi_k^{(L)}(x) + \sum_{j=L}^{-1} \sum_{k\in\mathbb{Z}} \tilde{d}_k^{(j)} \psi_k^{(j)}(x),$$
$$f_{\mathrm{PDF}}(x) \in L^2(\mathbb{R}) \tag{7}$$

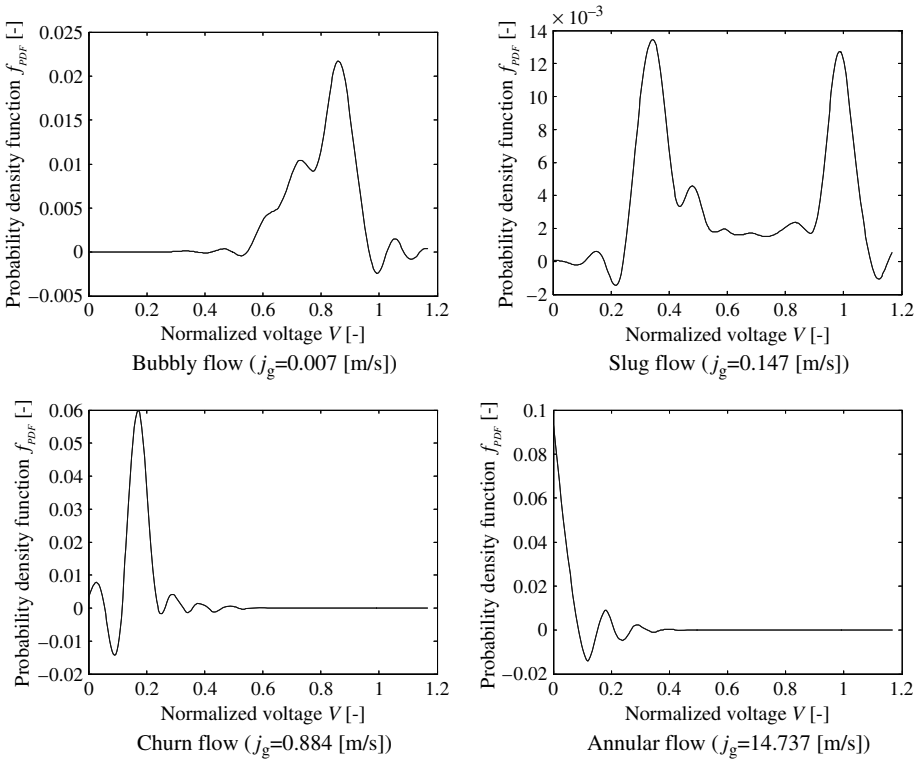

Figure 8. PDF obtained in each flow regime ($j_l = 0$ (m s^{-1})).

where j is the resolution level, L is the primary resolution level and k is the shift. The coefficients $\tilde{c}_k^{(L)}$ and $\tilde{d}_k^{(j)}$ are the estimators given by

$$\tilde{c}_k^{(L)} = \frac{1}{m}\sum_{i=1}^{m}\phi_k^{(L)}(X_i), \qquad \tilde{d}_k^{(j)} = \frac{1}{m}\sum_{i=1}^{m}\psi_k^{(j)}(X_i) \quad (8)$$

with the following two-scale relations:

$$\phi_k^{(L)}(x) = \sqrt{2^L}\,\phi(2^L x - k), \quad \phi(x) = \sum_{k\in\mathbb{Z}} p_k\,\phi(2x-k), \quad (9)$$

$$\psi_k^{(j)}(x) = \sqrt{2^j}\,\psi(2^j x - k), \quad \psi(x) = \sum_{k\in\mathbb{Z}} q_k\,\phi(2x-k), \quad (10)$$

where X_i is the sample of the ith bin and m is the number of bins ($m = 300$ in the present study). $\{p_k\}$ and $\{q_k\}$ are the two-scale sequences which are given according to wavelet [6] and $q_k = (-1)^k p_{1-k}$. The Daubechies wavelet (Daubechies 10) is used. The first term in equation (7) is the coarse approximation of the PDF and the second one is the detail of it. The PDF is estimated as the sum of the approximation and the detail of resolution level -5 (see figures 7(b) and (c)), namely

$$f_{\mathrm{PDF}}(x) \approx \sum_{k\in\mathbb{Z}} \tilde{c}_k^{(-5)}\phi_k^{(-5)}(x) + \sum_{k\in\mathbb{Z}} \tilde{d}_k^{(-5)}\psi_k^{(-5)}(x). \quad (11)$$

The estimated PDF is expected to contain the characteristics of the flow regimes as shown in figure 8. The 300 data for each PDF are grouped into 10 regions. In each region, the maximum value of data is found (see figures 7(c) and (d)). In this process, a set of 10 data is obtained for one PDF and is used as an input vector for the ANNs.

4. Results and discussion

In numerical experiments, we have tested several kinds of ANNs for the classification of flow regimes. As our result, we find that ANNs using a radial basis function (RBF) are effective for the present classification of flow regimes. The following RBF neural network is finally adopted:

$$y = \sum_{i=1}^{n} W_i^{\langle 2\rangle}\phi_{\mathrm{RBF}}\left(b_i^{\langle 1\rangle}\|\boldsymbol{p} - \boldsymbol{C}_i^{\langle 1\rangle}\|\right) + b^{\langle 2\rangle} \quad (12)$$

with

$$b_i^{\langle 1\rangle} = \frac{1}{\zeta}\phi_{\mathrm{RBF}}^{-1}(0.5) \quad (13)$$

where y is the output that indicates one of the flow regimes, $\boldsymbol{p}$ is the input vector obtained by the measurement, W is the weight and b is the bias. $A_i^{\langle l\rangle}$ stands for a value of A in the ith neuron of the lth layer. Here we gave $\boldsymbol{C}_i^{\langle 1\rangle} = \boldsymbol{p}_i^{\mathrm{tar}}$ by using a training set $\{(\boldsymbol{p}_i^{\mathrm{tar}}, y_i^{\mathrm{tar}})\}_{i=1}^{p}$, and then $n = p$. It is noted that t_i^{tar} is termed the 'target'. From the results of the visualization, the targets are assigned to flow regimes like 1 = 'bubbly', 2 = 'slug', 3 = 'churn' and 4 = 'annular'. ζ is the coefficient used to determine the width of the RBF. $W_i^{\langle 2\rangle}$ and $b^{\langle 2\rangle}$ can be uniquely determined by the training set $\{(\boldsymbol{p}_i^{\mathrm{tar}}, y_i^{\mathrm{tar}})\}_{i=1}^{p}$. ϕ_{RBF} is the radial basis function (RBF). Figure 9 presents the process used to find the output (flow regime) in the RBF neural network. The flow regimes (output vectors) corresponding to the input vectors can be expressed using functions of the input vectors. The RBF interpolates the input vectors of the training set to find the function. Hence, the

Table 2. Appropriate RBFs for the present method and resulting errors of the flow regime classification.

RBF	Gaussian $\phi_{\mathrm{RBF}} = \mathrm{e}^{-x^2}$	Cauchy $\phi_{\mathrm{RBF}} = \frac{1}{x^2+1^2}$	Multiquadric $\phi_{\mathrm{RBF}} = \sqrt{x^2+1^2}$	Inverse multiquadric $\phi_{\mathrm{RBF}} = \frac{1}{\sqrt{x^2+1^2}}$
Error	1.59%	1.59%	1.59%	1.19%

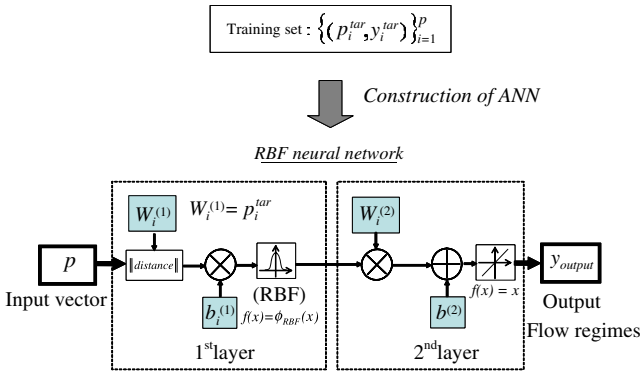

Figure 9. Structure of the RBF neural network.

RBF neural network works as the function. The classifications of flow regimes were performed with several types of RBF. The RBFs that can classify the flow regimes with relatively small errors are listed in table 2. The RBF neural network was constructed with 126 pairs of the training set, i.e., $p = 126$ and the investigation of the classification was performed with 252 input data. Table 2 also shows the resulting error for each RBF. As shown in table 2, the inverse multiquadric RBF resulted in the smallest error of 1.19%. The others could classify the flow regimes with the small error of 1.59%. Taking into account the results, it can be concluded that the present method is indeed effective for the classification of flow regimes.

5. Conclusions

A technique of classification of flow regimes in air–magnetic fluid two-phase flow is proposed using electromagnetic induction for data generation and supervised-training artificial neural networks for classification. A vertical upward two-phase flow is of interest. Our result is that the corresponding signals to flow regimes can be obtained by measurement using electromagnetic induction. To detect the characteristics of signals, the utilization of the wavelet transforms is effective. The RBF neural network is applicable for flow regime classification with an error of less than 1.6%. The smallest classification error 1.19% is obtained using the inverse multiquadric RBF.

Acknowledgment

This work was supported by a Grant-In-Aid for Scientific Research (C) from the Ministry of Education, Culture, Sports, Science and Technology, Japan.

References

[1] Sekoguchi K and Inoue K 1987 *JSME Int.* **30** 1266–73
[2] Hernandez L, Julia J E, Chiva S, Paranjape S and Ishii M 2006 *Meas. Sci. Technol.* **17** 1511–21
[3] Okubo M, Ishimoto J and Kamiyama S 1994 *Cavitation and Multiphase Flow ASME, FED* **194** 105–10
[4] Shuchi S, Mori T and Yamaguchi H 2002 *IEEE Trans. Magn.* **38** 3234–6
[5] Kuwahara T and Yamaguchi H 2007 *J. Thermophys. Heat Transfer* **21** 173–80
[6] Mallat S 1999 *A Wavelet Tour of Signal Processing* 2nd edn (San Diego, CA: Academic)
[7] Teolis A 1998 *Computational Signal Processing with Wavelets* (Boston, MA: Birkhäuser)